THE JOURNAL OF PHYSICAL CHEMISTRY C

Article

Cite This: J. Phys. Chem. C 2017, 121, 22690-22699

pubs.acs.org/JPCC

Linker Length-Dependent Electron-Injection Dynamics of Trimesitylporphyrins on SnO_2 Films

Shin Hee Lee,[‡] Kevin P. Regan,[‡] Svante Hedström,[§] Adam J. Matula, Subhajyoti Chaudhuri, Robert H. Crabtree,* Victor S. Batista,* Charles A. Schmuttenmaer,* and Gary W. Brudvig*

Department of Chemistry and Yale Energy Sciences Institute, Yale University, New Haven, Connecticut 06520-8107, United States

Supporting Information

ABSTRACT: Electron-injection dynamics of dye-sensitized photoelectrochemical cells depend on the length of the linker connecting the molecular photosensitizer to the metal oxide electron acceptor. However, systematic studies of the effect of chromophore−oxide distance are scarce. Here we present the synthesis, characterization, spectroscopy, and computational modeling of electron-injection dynamics from free-base trimesitylporphyrins with varying linker lengths into tin(IV) oxide (SnO_2). In each system, the porphyrin core and metal oxide film remain the same while only the linker binding the porphyrin to the carboxylate anchor group is varied. A length range spanning 8.5−17.2 Å is studied by employing phenylene, biphenylene, terphenylene, and benzanilide groups as the linker. We find a clear correlation between linker length and injection rates, providing insights that will be exploited in the optimization of dye-sensitized photoelectrochemical cells.

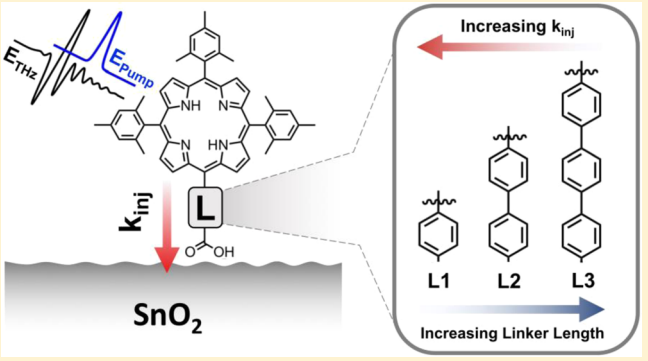

1. INTRODUCTION

Photoelectrochemical cells (PECs), which harvest energy from the sun to produce fuel, have experienced significant developments as an alternative energy source to fossil fuels.[1] The conversion of solar energy to a useable fuel requires the efficient capture of solar light followed by charge separation and a fuel-forming reaction as a means to store that energy. One strategy for addressing the challenges posed by both capture and conversion is a water-splitting dye-sensitized photoelectrochemical cell (WS-DSPEC), which oxidizes water via a catalyst at a photoanode to produce O_2 and reduces protons at the cathode to produce H_2.[2,3] The H_2 produced at the cathode is directly useable as an energy source and can be stored for later use.

One important step in WS-DSPECs is the photoinduced electron injection from a photosensitizer to the metal oxide. If the conduction band minimum (CBM) of the metal oxide material is at a lower energy than the lowest unoccupied molecular orbital (LUMO) of the photosensitizer, then a driving force exists for interfacial electron transfer into the conduction band of the metal oxide material.[4] Electron transfer occurs through the molecular linker/anchor portion of the photosensitizer, which is the connection between the chromophore core and the metal oxide.[5] A wealth of literature exists on photosensitizers for PECs, including ruthenium-based,[6−8] porphyrin-based,[9−11] and other organic dyes.[12−15] In this study, we employ porphyrin-based dyes because they possess broad absorbance across the visible region, have appropriate highest occupied molecular orbital (HOMO) energies for water-oxidation catalysis, and have appropriate LUMO energies for the injection of electrons into metal oxides. Furthermore, these porphyrins can be tailored synthetically as needed via the introduction of different functional or conjugating groups to the molecular structures.

Other studies have reported the influence of altering the porphyrin structural features on interfacial electron injection,[16−25] but we focus here on varying the linker group's length. In a WS-DSPEC, a photosensitizer and its accompanying water-oxidation catalyst must be positioned in close proximity such that the hole can be efficiently transferred to the catalyst. Therefore, it is desirable to match the height of the dye to the height of the catalyst above the surface.[26] The role of molecular linker lengths of donor−acceptor dyads and photosensitizers for electron-injection dynamics on metal oxide surfaces has been studied by other groups using various techniques, but not including terahertz spectroscopy.[22,27−36] Albinsson and co-workers observed an attenuating dependence of singlet energy-transfer rate on increasing porphyrin-dyad linker length using absorption and emission spectroscopies.[32] Lian and co-workers varied the linker lengths of Re complexes on SnO_2 films with methylene units and found a decrease in the injection rate with increasing linker length using femtosecond infrared spectroscopy.[34] However, there exists a gap in the literature in the use of terahertz spectroscopy coupled with computational modeling to study the relationship between linker length and electron-injection dynamics of free-base trimesityl porphyrins on SnO_2, a

Received: August 7, 2017
Published: September 21, 2017

DOI: 10.1021/acs.jpcc.7b07855
J. Phys. Chem. C 2017, 121, 22690−22699

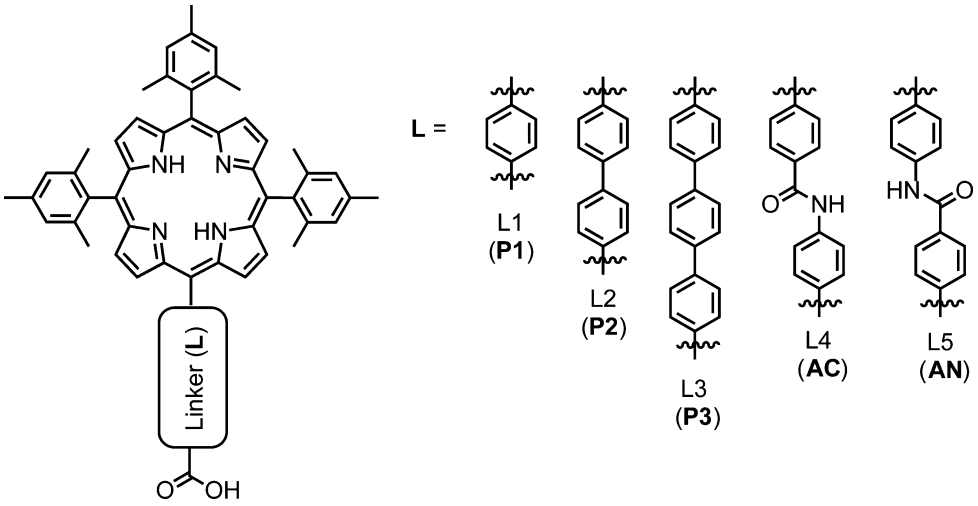

Figure 1. Molecular structures of trimesitylporphyrins used in this study.

metal oxide with appropriate energy levels for electron injection by high-potential porphyrins, which are promising photosensitizers for WS-DSPEC.[2,23] Herein, we discuss the synthesis, computational analysis, and characterization of electron-injection dynamics using terahertz (THz) spectroscopy of a series of five trimesitylporphyrins having varied molecular linker lengths (Figure 1). Three of these porphyrins (**P3, AC,** and **AN**) are new, and our novel synthetic methodologies are applicable to other porphyrin structures. Understanding the electron-injection dynamics of linkers with different lengths and properties will enable rational design and optimization of future porphyrin-based photosensitizers.

2. EXPERIMENTAL METHODS

2.1. Sample Preparation. All chemicals for synthesis were obtained commercially and used without further purification. For spectroscopic measurements, thin-film samples of each porphyrin on SnO_2 films were prepared in triplicate on 25 mm × 25 mm × 1 mm fused silica slides (GM Associates). A paste of SnO_2 nanoparticles with dimensions of 17−19 nm was prepared using a screen-printing paste procedure.[37] The fused silica slides were outlined with Scotch Magic tape as spacer and were doctor-bladed with SnO_2 paste, and then dried at 80 °C for 10 min in air. This step was repeated to produce two layers of SnO_2. The resulting films were sintered in a box furnace in air at 470 °C for 30 min. All SnO_2/quartz slides were sensitized in fresh 0.18 mM porphyrin solutions in dichloromethane for 9 h at room temperature in the dark.

2.2. Absorption and Emission. The steady-state absorption and emission spectra of ∼2 μM porphyrin solutions in a 1 cm × 1 cm quartz cuvette were obtained with a UV−visible spectrophotometer (Shimadzu UV-2600) and fluorometer (Horiba Scientific FluoroMax Plus), respectively. The emission spectra were acquired from 560 to 800 nm after exciting the porphyrins at 514 nm. The excited-state (S_1) potentials were estimated using the Rehm−Weller approximation.[23,38] Fluorescence quantum yields (Φ_F) were calculated using the equation:[39]

$$\Phi_F = \Phi_{ref}\left(\frac{A_{ref}}{A_s}\right)\left(\frac{I_s}{I_{ref}}\right)\left(\frac{\eta_s}{\eta_{ref}}\right)^2 \quad (1)$$

where the subscript *s* denotes the sample of interest, the subscript *ref* refers to the reference sample, A is the absorbance at the excitation wavelength, I is the integrated area of the emission spectra (Horiba Software), and η is the solvent refractive index.

2.3. Electrochemistry. Cyclic voltammetry (CV) measurements were conducted with a potentiostat (Pine WaveNow) in a three-electrode electrochemical cell using a glassy carbon working electrode, an Ag/AgCl wire pseudoreference electrode, and a platinum wire counter electrode. Carboxy-trimesitylporphyrins in dichloromethane (3 mM) were prepared for the experiments, and tetrabutylammonium hexafluorophosphate ($TBAPF_5$, 100 mM) in anhydrous dichloromethane was used as the supporting electrolyte. The glassy carbon electrode was polished with an alumina slurry in between each experiment. A ferrocenium/ferrocene redox couple was used as the internal standard to determine the potential of the pseudoreference electrode, which has an $E_{1/2}$ value of 0.690 V in dichloromethane versus normal hydrogen electrode (NHE).[40] All of the CVs were recorded at a scan rate of 50 mV/s and are referenced to the NHE.

2.4. Time-Resolved Terahertz Spectroscopy. Optical pump − THz probe spectroscopy (OPTP) was used to explore the ultrafast injection dynamics in trimesitylporphyrin/metal oxide systems. An ultrafast Ti:sapphire laser system (Spectra-Physics Spitfire Ace) which has a 4 W output of 800 nm light at 1 kHz repetition rate and a 35 fs pulse width was utilized.[2,5,41,42] The OPTP technique has been reported in many previous studies. The laser light is partitioned into the THz probe generation beam, the THz gate beam, and the optical pump beam. THz radiation is generated by focusing the 800 nm light and frequency-doubled 400 nm light into an air plasma source.[43] The THz gate beam tracks the amplitude of the THz probe as a function of probe delay, t_{probe}, which is done by free space electro-optical sampling in a zinc telluride (ZnTe ⟨110⟩) crystal.[44] The optical pump beam at 400 nm was generated from the fundamental 800 nm beam with a 500 μm thick Type 1 β-barium borate crystal (BBO, Eskima Optics).

THz radiation is attenuated in the presence of free carriers in the metal oxide material upon photoexcitation. The peak amplitude of the THz pulse is monitored at a fixed t_{probe} as a function of optical pump delay, t_{pump}. A mechanical delay stage allows for a time delay between the optical and THz pulses. Electron-injection dynamics were probed over a ∼1.8 ns time

DOI: 10.1021/acs.jpcc.7b07855
J. Phys. Chem. C 2017, 121, 22690−22699

window. All measurements were taken as a function of t_{pump}, as the difference between the photoexcited and nonphotoexcited sample.

2.5. Quantum Chemistry Calculations. Density functional theory (DFT) was used to optimize all dye structures in an implicit dichloromethane polarizable continuum solvent[45] at the B3LYP[46]/6-31G(df,p)[47] level of theory, using the Gaussian09 program.[48] Frequency calculations were then performed to ensure the minimum energy geometry was stable. Linear-response time-dependent (TD)-DFT calculations were performed to obtain the five lowest-energy electronic transitions for each dye. Single point calculations at the B3LYP/6-311+G(2df,p) level were then performed to obtain more accurate energetics and orbitals. This was repeated with unrestricted DFT for the singly oxidized states to obtain their spin isodensity plots. Structural optimizations of the excited S_1 state of the neutral dyes were carried out with TD-DFT in vacuum, corresponding to the OPTP experiments performed in air. Orbital and electron-density isosurfaces were generated with the Chimera software.[49]

Electron-injection calculations were performed, as previously described,[50−53] using a tight-binding Extended Hückel (EH) Hamiltonian that reproduces a SnO_2 bandgap of 3.6 eV (see Table S8 for details). The geometry of the benzoate anchor bound to SnO_2 was obtained by geometry optimization at the B3LYP/6-31G(df,p)[C,H,O]/Def2SV[Sn][54] level of theory, using a model system composed of the benzoate group covalently bound to a $Sn_{21}O_{42}$ cluster in a bidentate fashion. The adsorbate and the 13 SnO_2 atoms closest to the binding site were allowed to relax, while the rest of the system was fixed to preserve the geometry of the SnO_2 crystal. The acidic proton of the benzoic group was bound to a SnO_2 surface oxygen to retain overall charge neutrality. The partially optimized anchor + proton + cluster was inserted into a periodic $Sn_{72}O_{144}$ slab, followed by attachment of the dye molecules in their S_1-state minimum energy conformations. The simulations of interfacial electron transfer were performed after initialization of the wave packet in a 50−50% superposition of the dye LUMO and LUMO +1 states. Propagation with an integration time-step of 1 fs was performed for 2 ps. The SI contains images of the optimized model slab and full dye system as well as the EH LUMO, LUMO +1, and 50−50% initial absorption state for the **P1** dye (Figure S6) and the initial state for all five dyes (Figure S7). Absorbing potentials were placed on the edge Sn atoms to mimic a semi-infinite slab and prevent artificial recurrence events due to the finite size of the model system. The time-dependent survival probability was computed to quantify the electronic population of the dye.

3. RESULTS AND DISCUSSION

3.1. Molecular Design. The porphyrins synthesized for this study (Figure 1) are all *meso*-substituted porphyrins. These are very commonly used as photosensitizers[55] because of their relatively facile synthesis and the range of molecular structures which can be obtained by condensing pyrroles and aldehydes bearing the desired *meso*-substituent.[56] Specifically, these *meso*-porphyrins are "A3B" porphyrins, meaning that they have three identical (A3) substituents and one different one (B). In order to bind strongly to a metal oxide surface, a photosensitizer requires at least one linker-anchoring group.[57] For all dyes in this study, we include only one linker-anchoring group to ensure that electron injection occurs though a single pathway into the SnO_2. The chromophore properties are maintained while varying the linker because the *meso*-phenyl of the linker is almost perpendicular to the macrocycle, thereby decoupling the linker from the porphyrin ring. Trimesitylporphyrins are known to prevent intermolecular $\pi-\pi$ aggregation by virtue of steric repulsion between the porphyrin ring and the mesityl *ortho*-methyl groups, which causes them to adopt an orientation perpendicular to one another.[55] Unlike the findings of Sundström et al.,[22] we attribute all charge injection to occur through the conjugated linker and not via through-space injection which is due to the nature of the rigid anchor/linker systems chosen for this study. Aggregation can be a problem for purification as well as for the study of electron-injection dynamics by introducing other possible electron-transfer pathways. For **P1**, **P2**, and **P3**, nonfunctionalized phenylene units were employed in the linker to prevent side reactions during their synthesis and to maintain high solubility.

This series of linkers provides a platform to systematically investigate injection dynamics as a function of distance to the SnO_2 surface while maintaining a linear linker geometry of the photosensitizers relative to the surface. The lengths of **AC** and **AN** fall in-between **P2** and **P3**, and the amide moiety was inspired by our previous work on Mn-terpy catalysts[58] to study the role of conjugation in the linkers for these trimesitylporphyrins. The only difference between the two linkers is the orientation of the amide. This affects the electronic coupling and the orbital energy landscape because the carbonyl is electron withdrawing while the amine has an electron-donating effect on the adjacent π systems. 4-Carboxylic acid moieties are common photosensitizer-anchoring groups that were used for both series of the porphyrin/linkers in order to ensure robust adsorption on SnO_2 surfaces in solution and in air.

3.2. Synthesis. *a. Phenylene trimesityl porphyrins.* 5-(4-Methoxycarbonylphenyl)-10,15,20-tris(2,4,6-trimethylphenyl)-porphyrin (**P1**) was synthesized using a reported procedure.[59] Briefly, a 3:1 mixture of mesityl aldehyde and methyl 4-formylbenzoate was condensed with pyrrole with $BF_3{\cdot}OEt_2$. The resulting species were then oxidized with 2,3-dichloro-5,6-dicyanobenzoquinone (DDQ), using a procedure developed by Lindsey et al.,[60] and then hydrolyzed under basic conditions. 5-(4-Carboxybiphenyl)-10,15,20-tris(2,4,6-trimethylphenyl)-porphyrin (**P2**) and 5-(4-carboxytriphenyl)-10,15,20-tris(2,4,6-trimethylphenyl)porphyrin (**P3**) were synthesized using coupling reactions with the same precursor porphyrin **1** to produce an ample amount of material (Scheme 1). This precursor was then coupled under nitrogen with boronic esters **L2-BE** and **L3-BE**, having linkers of the desired lengths, to produce **P2-Ester** and **P3-Ester** in 80% and 87% yields, respectively. Hydrolysis of the two esters in basic aqueous conditions gave the desired final products **P2** and **P3** in 86% and 75% yields, respectively. Silica-based column chromatography was used to achieve high purity, a particular challenge for the carboxylic acid derivatives due to their favorable binding with the silica.

b. Synthesis of amide trimesityl porphyrins. The synthesis of 5-(4-carboxyphenylene-benzamido-phenyl)-10,15,20-tris(2,4,6-trimethylphenyl)porphyrin (**AC**) and 5-(4-carboxyphenylene-carbamoyl-phenyl)-10,15,20-tris(2,4,6-trimethylphenyl)-porphyrin (**AN**) did not involve Pd-catalyzed coupling reactions like the phenylene series of porphyrins in Scheme 1 due to the vulnerability of the amide groups in the linkers especially to strong basic conditions, making it difficult for preparing the boronic esters of the linkers (Scheme 2). Both **AC** and **AN** were made via deprotection of their esters that have *tert*-butyl protecting groups. The synthesis of **AC** began with the conversion of **P1** to an acyl chloride by modifying a procedure

DOI: 10.1021/acs.jpcc.7b07855
J. Phys. Chem. C 2017, 121, 22690−22699

Scheme 1. Synthesis of Bi- and Triphenylene Carboxytrimesitylporphyrins P2 and P3

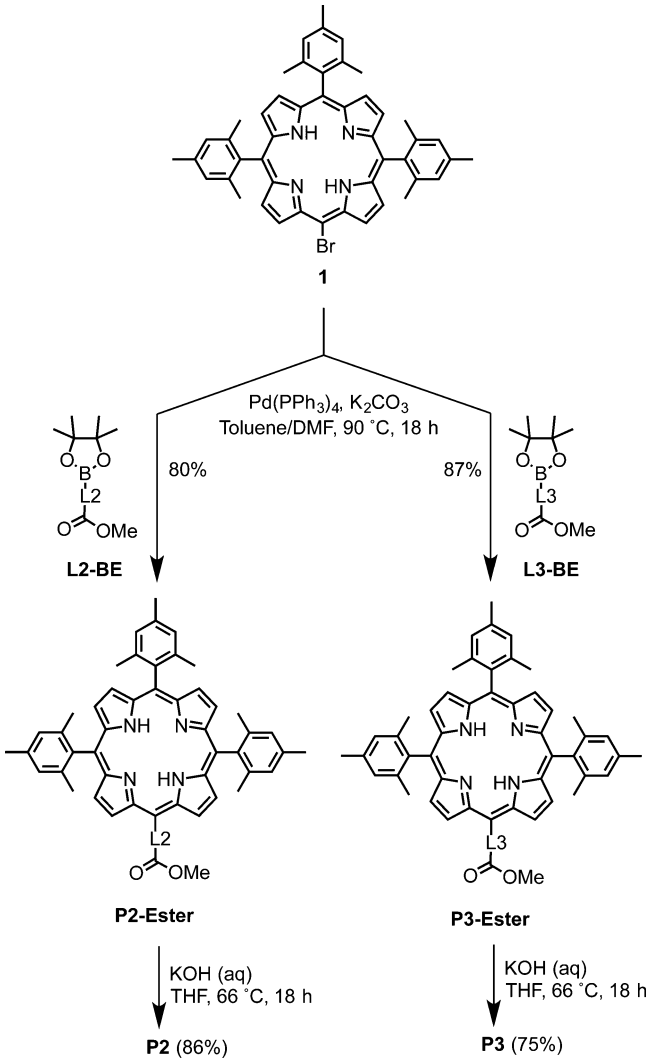

we reported,[61] which was then rapidly treated with *tert*-butyl 4-aminobenzoate in dichloromethane containing a small amount of pyridine to produce **AC-Ester** in 81% yield. For porphyrin **AN**, nitroporphyrin **2** was reduced to 5-(4-aminophenyl)-10,15,20-trimesitylporphyrin (**3**) using a reported procedure,[62] followed by coupling with 4-(*tert*-butoxycarbonyl)benzoic acid catalyzed by 1-ethyl-3-(3-(dimethylamino)propyl)carbodiimide (EDC) and 1-hydroxybenzotriazole hydrate (HOBt Hydrate) under ambient conditions to afford **AN-Ester** in 64% yield.

3.3. Photophysical and Electrochemical Properties. The measured steady-state absorption and emission spectra maxima values are listed in Table 1. All five trimesityl porphyrins **P1**, **P2**, **P3**, **AC**, and **AN** exhibited almost identical absorption peaks with an intense Soret band at around 419 nm and four Q-band peaks in the range 514 to 657 nm (Figure S3). In general for all porphyrins, the Soret band is a result of two intense $\pi-\pi^*$ transitions from the ground-state singlet (S_0) to an excited state pair collectively denoted S_2, while the Q-bands are due to two electronically excited states denoted S_1 (Q_x and Q_y), which in free-base porphyrins each show a 2-fold vibronic splitting. In addition to direct excitation from the ground state, the S_1 states can also be reached from an exothermic internal conversion process from S_2 following excitation in the Soret band. The character of these transitions as calculated by TD-DFT is listed for all dyes in Tables S2−S6 in the Supporting Information. The five porphyrins also have very similar fluorescence emission peaks, and the modest but consistent Stokes shifts have previously been rationalized from TD-DFT calculations showing structural relaxation of the excited state.[23] The absorption and emission peaks are unaffected by changing the linkers at the *meso*-positions, implying that the linkers do not affect the electronic structure of the porphyrin cores.

The absorption spectra of the five trimesitylporphyrins on SnO_2 surfaces are shown in Figure S3. The four peaks observed between 500 and 700 nm comprise the Q-band, and the superimposed spectra demonstrate that all peaks are identical across the series of dyes. This result confirms that the SnO_2 surfaces were sensitized with equal dye loading. When compared to the Q-band peaks of a representative trimesitylporphyrin in dichloromethane solution (not on SnO_2), the peak positions are unchanged, indicating little to no chromophore−surface interaction, e.g. by face-to-face π-aggregation.[63]

The results pertaining to the electrochemical properties of the five trimesitylporphyrins also show that the different linkers have an insignificant influence on the porphyrin ring system; all dyes have similar oxidative midpoint potentials ($E_{1/2}$) vs NHE (Figure S2). This is consistent with the highly uniform calculated absolute HOMO energies across the set, ranging from −5.44 eV to −5.51 eV vs vacuum (see Table S7). Because the photoexcited electron will be transferred from the porphyrin to the conduction band of SnO_2, the potential difference between the two represents the driving force for electron injection. The energy levels of the porphyrins were determined by obtaining the ground-state potentials of the porphyrin radical cation/porphyrin couple from the CV measurements and calculating the E_{0-0} values ($S_0 \rightarrow S_1$) from UV−visible spectroscopic measurements. Free-base porphyrins typically show E_{0-0} values of 1.92 eV, as all five of these dyes do (Table 1). The five porphyrins have similar estimated potentials of S_1 states that are well above the SnO_2 conduction band edge (~0.05 V vs NHE), which makes their electron-injections thermodynamically viable.

3.4. Electron-Injection Dynamics. Time-resolved THz spectroscopy is a unique tool for studying electron-injection and trapping dynamics in photosensitizer/metal oxide systems.[2,3,5,23,51,64] THz radiation is sensitive to the conductivity of photoinjected mobile electrons within the metal oxide's conduction band (CB). The transient conductivity of the material is proportional to the product of the photoinduced carrier mobility, μ, and the carrier density, N. Therefore, we monitor the population of photoinduced charge carriers as a function of optical pump delay, t_{pump}, with subpicosecond temporal resolution. When no mobile charges are in the CB, i.e. prior to photoexcitation, it is transparent to THz radiation. However, once the photosensitizer is photoexcited, mobile carriers are injected into the CB of the metal oxide, and those charges both reflect and scatter the THz radiation, which leads to a decrease in the THz transmission, ΔTHz.

In each porphyrin/metal oxide system, the trimesitylporphyrin is excited with 400 nm light at a pump fluence of 100 μJ/cm^2. The same trimesitylporphyrin photosensitizer core and carboxylic acid anchor group are used for each one. Only two quantities are varied: the length (**P1** < **P2** < **AC** < **AN** < **P3**), and the overall molecular conjugation and electronic effects due to the positioning of the nitrogen/oxygen groups of the linker (**P1, P2, P3** vs **AC, AN**).

DOI: 10.1021/acs.jpcc.7b07855
J. Phys. Chem. C 2017, 121, 22690−22699

Scheme 2. Synthesis of Trimesitylporphyrins AC and AN

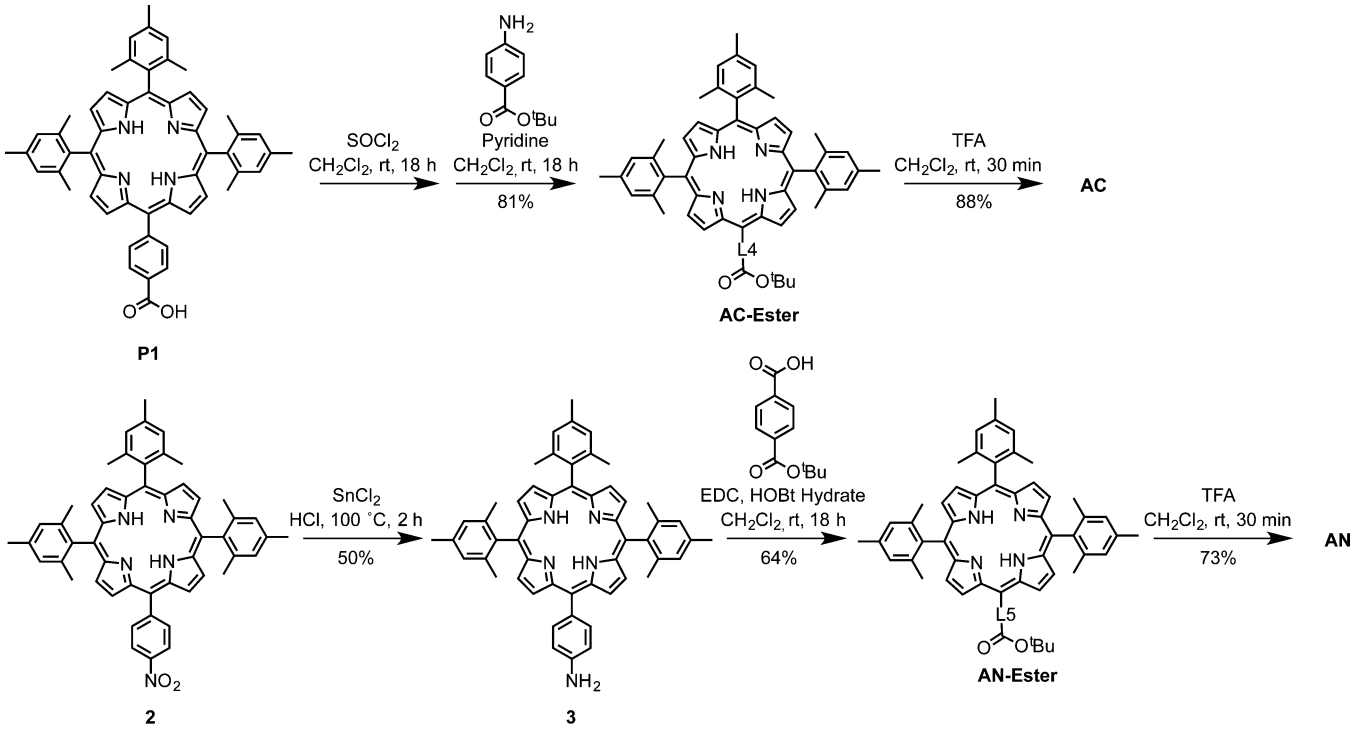

Table 1. Electrochemical and Photophysical Properties of Carboxy-Trimesitylporphyrins in Dichloromethane

Porphyrin	λ_{abs} (nm)	λ_{ems} (nm)	Φ_f [a]	first $E_{1/2}$ [b] (V vs NHE)	second $E_{1/2}$ [b] (V vs NHE)	E_{0-0} (eV)	S_1 [c] (V vs NHE)
P1	418, 514, 547, 590, 645	647, 714	0.082	1.23	1.70	1.92	−0.69
P2	419, 515, 549, 590, 646	648, 715	0.092	1.20	1.73	1.92	−0.72
P3	419, 515, 549, 590, 647	649, 716	0.088	1.22	1.70	1.92	−0.70
AC	418, 514, 548, 590, 645	647, 714	0.084	1.28	1.77	1.92	−0.64
AN	419, 514, 549, 590, 646	649, 714	0.088	1.21	1.74	1.92	−0.71

[a]Determined in toluene relative to tetramesitylporpyrin in toluene (Φ_f = 0.088). [b]Midpoint potentials determined by cyclic voltammetry. [c]First excited state potentials determined by subtracting E_{0-0} (Figure S1) from 1st $E_{1/2}$.

Lian et al. previously studied the electron-injection rates of a rhenium-based photosensitizer attached to TiO_2 as a function of molecular linker lengths by inserting CH_2 spacers using fs-transient mid-IR spectroscopy.[65] They observed a nonlinear trend in the injection rate as a function of length by monitoring intraband transitions, free carrier absorption, and absorption of trap states. On the other hand, we directly measure mobile electrons within the metal oxide's CB.[65,66] Therefore, we monitor the overall time scales of injection from the singlet states (both S_1 and S_2) into the CB of SnO_2.[2,5,23] Figure 2 presents the OPTP traces of dye-sensitized films on SnO_2 while varying the length of the linkage between the trimesitylporphyrin and the carboxylate anchor. The lengths of **P1** (8.58 Å), **P2** (12.91 Å), **P3** (17.24 Å), **AC** (15.04 Å), and **AN** (15.11 Å) were determined through ground state electronic structure geometry optimizations (Figure S8). These distances are measured from the DFT-optimized structures as the distance between the meso-carbon at the edge of the porphyrin ring and the anchor carbonyl carbon and adding it to the distance between the anchoring oxygen atoms and the nearest Sn atom.

The OPTP transients are well-described by a biexponential injection rate (k_1, k_2) and a single exponential trapping rate (k_{trap}), which is described as[5,23]

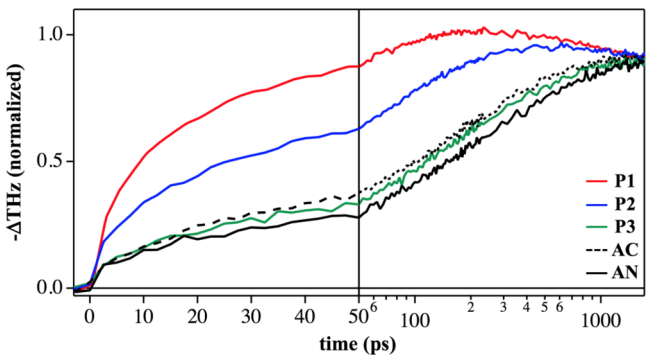

Figure 2. OPTP traces of **P1** (red), **P2** (blue), **P3** (green), **AC** (dashed black), and **AN** (solid black) are normalized based on their best fit amplitudes from eq 2 to compare the overall ultrafast dynamics as a function of linker length. In each case, the porphyrin was photoexcited with 400 nm light at a fluence of 100 $\mu J/cm^2$.

$$-\Delta THz = [A_1(1 - e^{-tk_1}) + A_2(1 - e^{-tk_2}) - (A_1 + A_2)(e^{-tk_{trap}} - 1)] \otimes G_R(FWHM) \quad (2)$$

The two injection rates have amplitudes A_1 and A_2, while the amplitude of trapping, A_{trap}, is the sum of A_1 and A_2. This ensures

DOI: 10.1021/acs.jpcc.7b07855
J. Phys. Chem. C 2017, 121, 22690−22699

that $-\Delta THz \rightarrow 0$ as $t \rightarrow \infty$. During best-fit optimization, the injection and trapping dynamics are convoluted with a Gaussian instrument response function that corresponds to 500 fs (full-width at half-maximum). Best-fit parameters along with standard deviations are given in Table S1, and the injection rates, k_1 and k_2, are plotted against linker length in Figure 3.

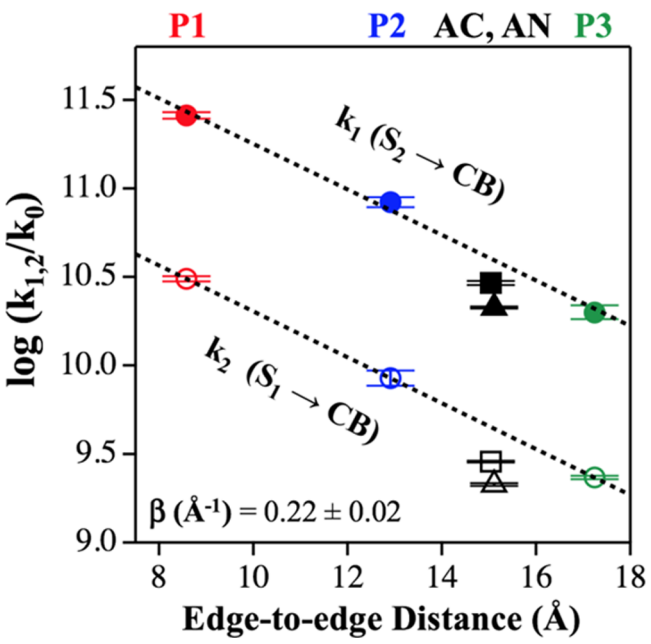

Figure 3. Plot of the common log of the extracted rate constants k_1 and k_2 versus edge-to-edge distance. Their associated standard deviations are displayed as well. The best fit lines for **P1**, **P2**, and **P3** are shown with dotted black lines.

Electron-transfer rates are often interpreted in the context of Marcus theory in the weak coupling limit (i.e., where $V \ll k_b T$).[67] Under equilibrium conditions ($\Delta G^\circ = 0$), the rate of electron transfer from the donor (trimesitylporphyrin) to the acceptor (CB of SnO_2) can be modeled, as follows:

$$k = \frac{2\pi}{\hbar} |V|^2 \frac{1}{\sqrt{4\pi\lambda k_b T}} \exp\left(-\frac{\lambda}{4k_b T}\right) \quad (3)$$

where k is the electron transfer rate, λ is the reorganization energy, k_b is the Boltzmann constant, T is the temperature in Kelvin, and V is the electronic coupling. The electronic coupling is typically exponentially dependent on the donor and acceptor distance, R,[67,68]

$$V = V_0 \exp\left(\frac{-\beta(R - R_0)}{2}\right) \quad (4)$$

where R_0 is the donor−acceptor van der Waals separation, and β is the electron tunneling scalar. β is an important metric that constitutes an overall measure of the conjugation in the donor−acceptor bridge. It ranges from 0 $Å^{-1}$ in a fully conjugated system to 2.8 $Å^{-1}$ in vacuum.[69] Due to the similar absorbance traces of each porphyrin, we assume that the reorganization energy, λ, and ΔG are independent of molecular linker length, eq 3 can be simplified to depend only on donor−acceptor distance and the β parameter:

$$k \propto V^2 \propto V_0^2 \exp(-\beta(R - R_0)) \quad (5)$$

Using this relation, the best-fit rates obtained from eq 5 are plotted as a function of edge-to-edge distance between the electron donor and acceptor, as seen in Figure 3. Due to the similarity of **P1**, **P2**, and **P3**, it is expected that the only factor differentiating the electron-transfer rates between them would be the effective distance between the donor and acceptor groups. That is, the conjugation strength remains nearly identical with the addition of phenylene rings from phenylene, to biphenylene, to terphenylene. Therefore, when the common logarithm of rates k_1 and k_2 is plotted as a function of edge-to-edge distance between donor and acceptor, the relationship is linear. The slope of the best-fit line determines the β parameter.

Not surprisingly, the β parameters for injection from the S_1 and S_2 state were statistically indistinguishable. While **P1**, **P2**, and **P3** show similar conjugation, **AC** and **AN** differ slightly due to their amide group in the molecular linker. Ultrafast electron-injection dynamics do not show a large difference between **AC** and **AN**, which indicates that the charge-injection rate is not significantly affected by the amide orientation of the linker for the trimesitylporphyrins within our system. The similarity between injection rates for **AC** and **AN** differs from our past studies where the amide group was directly attached to the photosensitizer core.[51] This difference arises because the extra phenyl ring between the porphyrin core and the amide group prevents direct interaction of the relevant porphyrin core orbitals. Finally, the rate of trapping, k_{trap}, is not influenced by the molecular linker length. It was globally fit and found to be 6.25×10^7 s^{-1}, which is consistent with our past work on dye-sensitized SnO_2.[64]

3.5. Computational Analysis. The electronic and optical properties calculated with DFT and TD-DFT are broadly in agreement with experiments (see Tables S2−S6 in the Supporting Information). The calculated orbital energies and electronic transitions verify that the linker has a limited effect on the porphyrin-centered Gouterman[70] orbitals HOMO−1, HOMO, LUMO, and LUMO+1. These frontier orbitals are shown in Figure 4 for representative dye **P1**, along with the meso-substituent-centered HOMO−2 and LUMO+2. Figure 4 also shows the calculated spin density of the singly oxidized form of **P1**. The correspondence to the HOMO shows that oxidizing the porphyrin effectively removes an electron from the HOMO. The frontier orbitals for the remaining four dyes are shown in Figure S5. For these molecules, the HOMO−2 and LUMO+2 show a small degree of variance stemming from the differing linkers.

Electron-injection dynamics simulations based on a tight-binding Extended Hückel (EH) Hamiltonian were performed with the wave packet initialized in LUMO and LUMO+1, the target orbitals for excitations in both the Q and Soret absorption bands (see Table S2−S6). Figure 5 shows the results of the simulated injection dynamics, where the trends largely agree with the experimental OPTP results (Figure 2). In absolute terms, the calculations overestimate the injection rate due to known limitations of the semiempirical method.[51] Nevertheless, in both experiments and simulations, **AC** and **P3** exhibit similar relaxation dynamics, while the **P** series shows a successive decrease in injection rate with increasing linker length, consistent with previous studies on porphyrin-to-SnO_2 injection.[50]

The calculated injection rate of **AN**, on the other hand, is overestimated relative to the other dyes. In **AN**, the π^* band of the carbonyl−benzoate part of the linker is stabilized slightly by the electron-withdrawing carbonyl, making the movement of electron density into this region more thermodynamically favorable and promoting the general movement of density

DOI: 10.1021/acs.jpcc.7b07855
J. Phys. Chem. C 2017, 121, 22690−22699

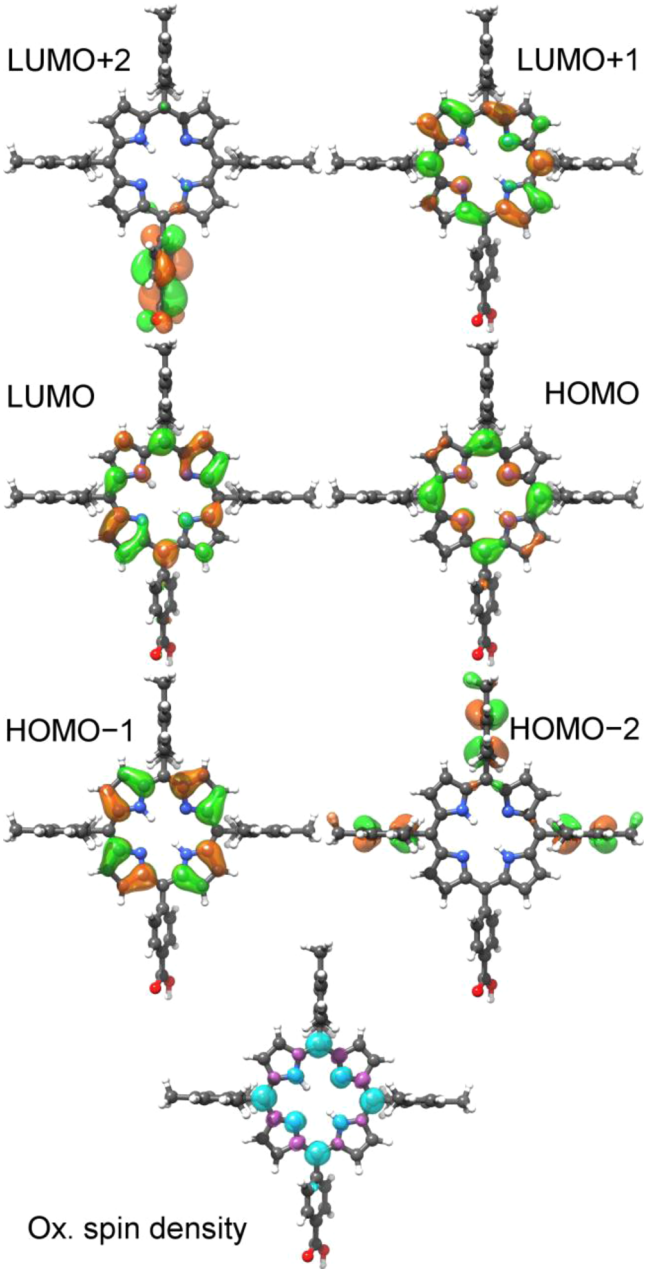

Figure 4. DFT frontier orbitals of **P1** (top) and the spin density of the singly oxidized state (bottom), where cyan and magenta represent spin up and down, respectively. Analogous isodensity plots for the other dyes are found in Figure S5.

toward the anchor and the semiconductor. The stabilization of the linker π^* band in **AN** is reflected in a very deep LUMO+2 orbital (Figure S5 and Table S7), and its LUMO delocalization is visualized in Figure S5. In our EH calculations, this π^* stabilization is greatly overestimated when compared to DFT, leading to the unphysically fast injection calculated for the **AN** system; see Table S9.

4. CONCLUSION AND OUTLOOK

A series of five trimesitylporphyrins have been synthesized and probed using ultrafast spectroscopy to determine the role of molecular linker length and conjugation in regard to the rate of electron injection from the singlet states (S_1 and S_2). Our studies have demonstrated that the porphyrin/linker/anchor/metal oxide systems have an exponential relationship between interfacial electron-injection rates and the porphyrin−surface distance.

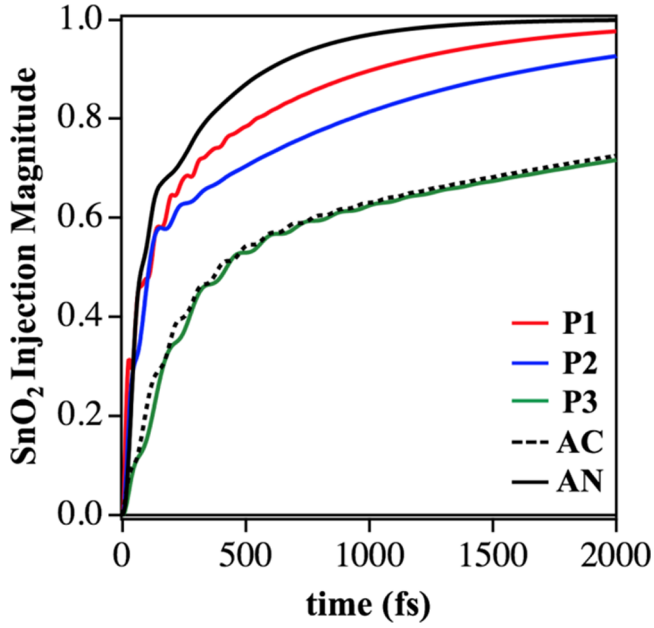

Figure 5. Extended Hückel electron-dynamics results showing the increase over time of the wave packet (WP) population on the SnO_2.

The **P1**, **P2**, and **P3** linkers exhibit an electronic coupling factor (β) of 0.22 ± 0.02 Å^{-1}, which is consistent with what would be expected from Marcus theory in the limit of weak electronic coupling. The injection rates of **AC** and **AN** are lower than the trend established by the **P** series, likely due to their decreased conjugation strength. The lower injection rates are attributed to charge-transfer barriers in the amide linkers which are likely due to their lack of conjugation and also to their phenylene components. DFT calculations of optoelectronic properties emphasize the important role of the frontier orbitals (HOMO−1 through LUMO+1). Simulations of interfacial electron-transfer dynamics enabled characterization of the injection process at the molecular level, yielding relative injection trends in good agreement with experiments. Future efforts will focus on studying the pH, solvent, and temperature-dependent effects on the electron-injection rates with varying linker length.

■ ASSOCIATED CONTENT

Supporting Information

The Supporting Information is available free of charge on the ACS Publications website at DOI: 10.1021/acs.jpcc.7b07855.

Synthesis, characterization, and electrochemical and computational details of the reported carboxy-trimesitylporphyrins (PDF)

■ AUTHOR INFORMATION

Corresponding Authors

*R.H.C.: Phone: 203-200-8936. E-mail: robert.crabtree@yale.edu.

*V.S.B.: Phone: 203-432-6672 victor.batista@yale.edu.

*C.A.S.: Phone: 203-432-5049. E-mail: charles.schmuttenmaer@yale.edu.

*G.W.B.: Phone: 203-432-5202. E-mail: gary.brudvig@yale.edu.

DOI: 10.1021/acs.jpcc.7b07855
J. Phys. Chem. C 2017, 121, 22690−22699

ORCID

Kevin P. Regan: 0000-0003-3522-092X
Svante Hedström: 0000-0001-6496-6865
Robert H. Crabtree: 0000-0002-6639-8707
Victor S. Batista: 0000-0002-3262-1237
Charles A. Schmuttenmaer: 0000-0001-9992-8578
Gary W. Brudvig: 0000-0002-7040-1892

Present Address

[§](S.H.) Department of Physics, Stockholm University, 10691 Stockholm, Sweden.

Author Contributions

[‡]S.H.L. and K.P.R. contributed equally.

Notes

The authors declare no competing financial interest.

■ ACKNOWLEDGMENTS

We thank the staff at Yale West Campus Analytical Core, Yale Chemical and Biophysical Instrumentation Center, and Yale WM Keck Foundation Biotechnology Resource Laboratory for their help with instrumentation. This work was supported by the U.S. Department of Energy, Chemical Sciences, Geosciences, and Biosciences Division, Office of Basic Energy Sciences, Office of Science (Grant DEFG02-07ER15909). Additional support was provided by a generous donation from the TomKat Charitable Trust. V.S.B. acknowledges computational time from NERSC and Yale HPC.

■ REFERENCES

(1) Moore, G. F.; Brudvig, G. W. Energy Conversion in Photosynthesis: A Paradigm for Solar Fuel Production. *Annu. Rev. Condens. Matter Phys.* **2011**, *2*, 303−327.

(2) Milot, R. L.; Schmuttenmaer, C. A. Electron Injection Dynamics in High-Potential Porphyrin Photoanodes. *Acc. Chem. Res.* **2015**, *48*, 1423−1431.

(3) Young, K. J.; Martini, L. A.; Milot, R. L.; Snoeberger, R. C., III; Batista, V. S.; Schmuttenmaer, C. A.; Crabtree, R. H.; Brudvig, G. W. Light-Driven Water Oxidation for Solar Fuels. *Coord. Chem. Rev.* **2012**, *256*, 2503−2520.

(4) Swierk, J. R.; Mallouk, T. E. Design and Development of Photoanodes for Water-Splitting Dye-Sensitized Photoelectrochemical Cells. *Chem. Soc. Rev.* **2013**, *42*, 2357−2387.

(5) Milot, R. L.; Moore, G. F.; Crabtree, R. H.; Brudvig, G. W.; Schmuttenmaer, C. A. Electron Injection Dynamics from Photoexcited Porphyrin Dyes into SnO_2 and TiO_2 Nanoparticles. *J. Phys. Chem. C* **2013**, *117*, 21662−21670.

(6) Bomben, P. G.; Robson, K. C. D.; Koivisto, B. D.; Berlinguette, C. P. Cyclometalated Ruthenium Chromophores for the Dye-Sensitized Solar Cell. *Coord. Chem. Rev.* **2012**, *256*, 1438−1450.

(7) Teuscher, J.; Décoppet, J.-D.; Punzi, A.; Zakeeruddin, S. M.; Moser, J.-E.; Grätzel, M. Photoinduced Interfacial Electron Injection Dynamics in Dye-Sensitized Solar Cells under Photovoltaic Operating Conditions. *J. Phys. Chem. Lett.* **2012**, *3*, 3786−3790.

(8) Kinoshita, T.; Dy, J. T.; Uchida, S.; Kubo, T.; Segawa, H. Wideband Dye-Sensitized Solar Cells Employing a Phosphine-Coordinated Ruthenium Sensitizer. *Nat. Photonics* **2013**, *7*, 535−539.

(9) Kang, S. H.; Choi, I. T.; Kang, M. S.; Eom, Y. K.; Ju, M. J.; Hong, J. Y.; Kang, H. S.; Kim, H. K. Novel D-π-A Structured Porphyrin Dyes with Diphenylamine Derived Electron-Donating Substituents for Highly Efficient Dye-Sensitized Solar Cells. *J. Mater. Chem. A* **2013**, *1*, 3977−3982.

(10) Yella, A.; Lee, H.-W.; Tsao, H. N.; Yi, C.; Chandiran, A. K.; Nazeeruddin, M. K.; Diau, E. W.-G.; Yeh, C.-Y.; Zakeeruddin, S. M.; Grätzel, M. Porphyrin-Sensitized Solar Cells with Cobalt(II/III)−Based Redox Electrolyte Exceed 12% Efficiency. *Science* **2011**, *334*, 629−634.

(11) Campbell, W. M.; Burrell, A. K.; Officer, D. L.; Jolley, K. W. Porphyrins as Light Harvesters in the Dye-Sensitised TiO_2 Solar Cell. *Coord. Chem. Rev.* **2004**, *248*, 1363−1379.

(12) Hara, K.; et al. Novel Conjugated Organic Dyes for Efficient Dye-Sensitized Solar Cells. *Adv. Funct. Mater.* **2005**, *15*, 246−252.

(13) Pei, K.; Wu, Y.; Islam, A.; Zhang, Q.; Han, L.; Tian, H.; Zhu, W. Constructing High-Efficiency D−A−π−A-Featured Solar Cell Sensitizers: a Promising Building Block of 2,3-Diphenylquinoxaline for Antiaggregation and Photostability. *ACS Appl. Mater. Interfaces* **2013**, *5*, 4986−4995.

(14) Hua, Y.; Chang, S.; Huang, D.; Zhou, X.; Zhu, X.; Zhao, J.; Chen, T.; Wong, W.-Y.; Wong, W.-K. Significant Improvement of Dye-Sensitized Solar Cell Performance Using Simple Phenothiazine-Based Dyes. *Chem. Mater.* **2013**, *25*, 2146−2153.

(15) Ragoussi, M.-E.; Ince, M.; Torres, T. Recent Advances in Phthalocyanine-Based Sensitizers for Dye-Sensitized Solar Cells. *Eur. J. Org. Chem.* **2013**, *2013*, 6475−6489.

(16) Hart, A. S.; Kc, C. B.; Gobeze, H. B.; Sequeira, L. R.; D'Souza, F. Porphyrin-Sensitized Solar Cells: Effect of Carboxyl Anchor Group Orientation on the Cell Performance. *ACS Appl. Mater. Interfaces* **2013**, *5*, 5314−5323.

(17) Martini, L. A.; Moore, G. F.; Milot, R. L.; Cai, L. Z.; Sheehan, S. W.; Schmuttenmaer, C. A.; Brudvig, G. W.; Crabtree, R. H. Modular Assembly of High-Potential Zinc Porphyrin Photosensitizers Attached to TiO_2 with a Series of Anchoring Groups. *J. Phys. Chem. C* **2013**, *117*, 14526−14533.

(18) Devaraj, N. K.; Decreau, R. A.; Ebina, W.; Collman, J. P.; Chidsey, C. E. D. Rate of Interfacial Electron Transfer through the 1,2,3-Triazole Linkage. *J. Phys. Chem. B* **2006**, *110*, 15955−15962.

(19) Auwarter, W.; Ecija, D.; Klappenberger, F.; Barth, J. V. Porphyrins at Interfaces. *Nat. Chem.* **2015**, *7*, 105−120.

(20) Eu, S.; Hayashi, S.; Umeyama, T.; Oguro, A.; Kawasaki, M.; Kadota, N.; Matano, Y.; Imahori, H. Effects of 5-Membered Heteroaromatic Spacers on Structures of Porphyrin Films and Photovoltaic Properties of Porphyrin-Sensitized TiO_2 Cells. *J. Phys. Chem. C* **2007**, *111*, 3528−3537.

(21) Griffith, M. J.; Sunahara, K.; Wagner, P.; Wagner, K.; Wallace, G. G.; Officer, D. L.; Furube, A.; Katoh, R.; Mori, S.; Mozer, A. J. Porphyrins for Dye-Sensitised Solar Cells: New Insights into Efficiency-Determining Electron Transfer Steps. *Chem. Commun.* **2012**, *48*, 4145−4162.

(22) Ye, S.; et al. Role of Adsorption Structures of Zn-Porphyrin on TiO_2 in Dye-Sensitized Solar Cells Studied by Sum Frequency Generation Vibrational Spectroscopy and Ultrafast Spectroscopy. *J. Phys. Chem. C* **2013**, *117*, 6066−6080.

(23) Jiang, J.; Swierk, J. R.; Materna, K. L.; Hedström, S.; Lee, S. H.; Crabtree, R. H.; Schmuttenmaer, C. A.; Batista, V. S.; Brudvig, G. W. High-Potential Porphyrins Supported on SnO_2 and TiO_2 Surfaces for Photoelectrochemical Applications. *J. Phys. Chem. C* **2016**, *120*, 28971−28982.

(24) Nayak, A.; Roy, S.; Sherman, B. D.; Alibabaei, L.; Lapides, A. M.; Brennaman, M. K.; Wee, K.-R.; Meyer, T. J. Phosphonate-Derivatized Porphyrins for Photoelectrochemical Applications. *ACS Appl. Mater. Interfaces* **2016**, *8*, 3853−3860.

(25) Moore, G. F.; Konezny, S. J.; Song, H.-e.; Milot, R. L.; Blakemore, J. D.; Lee, M. L.; Batista, V. S.; Schmuttenmaer, C. A.; Crabtree, R. H.; Brudvig, G. W. Bioinspired High-Potential Porphyrin Photoanodes. *J. Phys. Chem. C* **2012**, *116*, 4892−4902.

(26) Brennan, B. J.; Regan, K. P.; Durrell, A. C.; Schmuttenmaer, C. A.; Brudvig, G. W. Solvent Dependence of Lateral Charge Transfer in a Porphyrin Monolayer. *ACS Energy Lett.* **2017**, *2*, 168−173.

(27) Guo, M.; Li, M.; Dai, Y.; Shen, W.; Peng, J.; Zhu, C.; Lin, S. H.; He, R. Exploring the Role of Varied-Length Spacers in Charge Transfer: a Theoretical Investigation on Pyrimidine-Bridged Porphyrin Dyes. *RSC Adv.* **2013**, *3*, 17515−17526.

(28) Lin, C.-Y.; Lo, C.-F.; Luo, L.; Lu, H.-P.; Hung, C.-S.; Diau, E. W.-G. Design and Characterization of Novel Porphyrins with Oligo-(phenylethylnyl) Links of Varied Length for Dye-Sensitized Solar Cells:

DOI: 10.1021/acs.jpcc.7b07855
J. Phys. Chem. C 2017, 121, 22690−22699

Synthesis and Optical, Electrochemical, and Photovoltaic Investigation. *J. Phys. Chem. C* **2009**, *113*, 755−764.
(29) Tan, C.-J.; Yang, C.-S.; Sheng, Y.-C.; Amini, H. W.; Tsai, H.-H. G. Spacer Effects of Donor-π Spacer-Acceptor Sensitizers on Photophysical Properties in Dye-Sensitized Solar Cells. *J. Phys. Chem. C* **2016**, *120*, 21272−21284.
(30) Myahkostupov, M.; Piotrowiak, P.; Wang, D.; Galoppini, E. Ru(II)-Bpy Complexes Bound to Nanocrystalline TiO_2 Films through Phenyleneethynylene (OPE) Linkers: Effect of the Linkers Length on Electron Injection Rates. *J. Phys. Chem. C* **2007**, *111*, 2827−2829.
(31) Kilså, K.; Kajanus, J.; Macpherson, A. N.; Mårtensson, J.; Albinsson, B. Bridge-Dependent Electron Transfer in Porphyrin-Based Donor−Bridge−Acceptor Systems. *J. Am. Chem. Soc.* **2001**, *123*, 3069−3080.
(32) Pettersson, K.; Kyrychenko, A.; Rönnow, E.; Ljungdahl, T.; Mårtensson, J.; Albinsson, B. Singlet Energy Transfer in Porphyrin-Based Donor−Bridge−Acceptor Systems: Interaction between Bridge Length and Bridge Energy. *J. Phys. Chem. A* **2006**, *110*, 310−318.
(33) Lu, X.; Shao, Y.; Wei, S.; Zhao, Z.; Li, K.; Guo, C.; Wang, W.; Zhang, M.; Guo, W. Effect of the Functionalized π-bridge on Porphyrin Sensitizers for Dye-sensitized Solar Cells: An in-depth Analysis of Electronic Structure, Spectrum, Excitation, and Intramolecular Electron Transfer. *J. Mater. Chem. C* **2015**, *3*, 10129−10139.
(34) Anderson, N. A.; Ai, X.; Chen, D.; Mohler, D. L.; Lian, T. Bridge-Assisted Ultrafast Interfacial Electron Transfer to Nanocrystalline SnO_2 Thin Films. *J. Phys. Chem. B* **2003**, *107*, 14231−14239.
(35) Imahori, H.; et al. Photoinduced Charge Carrier Dynamics of Zn−Porphyrin−TiO_2 Electrodes: The Key Role of Charge Recombination for Solar Cell Performance. *J. Phys. Chem. A* **2011**, *115*, 3679−3690.
(36) Galoppini, E.; Guo, W.; Zhang, W.; Hoertz, P. G.; Qu, P.; Meyer, G. J. Long-Range Electron Transfer across Molecule−Nanocrystalline Semiconductor Interfaces Using Tripodal Sensitizers. *J. Am. Chem. Soc.* **2002**, *124*, 7801−7811.
(37) Antoniuk-Pablant, A.; Terazono, Y.; Brennan, B. J.; Sherman, B. D.; Megiatto, J. D.; Brudvig, G. W.; Moore, A. L.; Moore, T. A.; Gust, D. A New Method for the Synthesis of β-Cyano Substituted Porphyrins and their use as Sensitizers in Photoelectrochemical Devices. *J. Mater. Chem. A* **2016**, *4*, 2976−2985.
(38) Rehm, D.; Weller, A. Kinetics of Fluorescence Quenching by Electron and H-Atom Transfer. *Isr. J. Chem.* **1970**, *8*, 259−271.
(39) Rochford, J.; Chu, D.; Hagfeldt, A.; Galoppini, E. Tetrachelate Porphyrin Chromophores for Metal Oxide Semiconductor Sensitization: Effect of the Spacer Length and Anchoring Group Position. *J. Am. Chem. Soc.* **2007**, *129*, 4655−4665.
(40) Sawyer, D. T. S., Andrzej; Roberts, Julian, L. *Electrochemistry for Chemists*, 2nd ed.; Wiley-Interscience: 1995.
(41) Regan, K. P.; Koenigsmann, C.; Sheehan, S. W.; Konezny, S. J.; Schmuttenmaer, C. A. Size-Dependent Ultrafast Charge Carrier Dynamics of WO_3 for Photoelectrochemical Cells. *J. Phys. Chem. C* **2016**, *120*, 14926−14933.
(42) Beard, M. C.; Turner, G. M.; Schmuttenmaer, C. A. Transient Photoconductivity in GaAs as Measured by Time-Resolved Terahertz Spectroscopy. *Phys. Rev. B: Condens. Matter Mater. Phys.* **2000**, *62*, 15764−15777.
(43) Kress, M.; Löffler, T.; Eden, S.; Thomson, M.; Roskos, H. G. Terahertz-pulse Generation by Photoionization of Airwith Laser Pulses Composed of Both Fundamental and Second-harmonic Waves. *Opt. Lett.* **2004**, *29*, 1120−1122.
(44) Wu, Q.; Zhang, X. C. Freespace Electrooptic Sampling of Terahertz Beams. *Appl. Phys. Lett.* **1995**, *67*, 3523−3525.
(45) Cancès, E. A New Integral Equation Formalism for the Polarizable Continuum Model: Theoretical Background and Applications to Isotropic and Anisotropic Dielectrics. *J. Chem. Phys.* **1997**, *107*, 3032−3041.
(46) Becke, A. D. Density-functional thermochemistry. III. The role of exact exchange. *J. Chem. Phys.* **1993**, *98*, 5648−5652.
(47) Ditchfield, R. H., Hehre, W. J.; Pople, J. A., Self-Consistent Molecular-Orbital Methods. IX. An Extended Gaussian-Type Basis for Molecular-Orbital Studies of Organic Molecules. 1971, *54*, 724−728.
(48) Frisch, M. J., et al. *Gaussian 09*, Revision B.01; Wallingford, CT, 2009.
(49) Pettersen, E. F.; Goddard, T. D.; Huang, C. C.; Couch, G. S.; Greenblatt, D. M.; Meng, E. C.; Ferrin, T. E. UCSF Chimera—A Visualization System for Exploratory Research and Analysis. *J. Comput. Chem.* **2004**, *25*, 1605−1612.
(50) Poddutoori, P. K.; Thomsen, J. M.; Milot, R. L.; Sheehan, S. W.; Negre, C. F. A.; Garapati, V. K. R.; Schmuttenmaer, C. A.; Batista, V. S.; Brudvig, G. W.; van der Est, A. Interfacial Electron Transfer in Photoanodes Based on Phosphorus(V) Porphyrin Sensitizers Co-deposited on SnO_2 with the Ir(III)Cp* Water Oxidation Precatalyst. *J. Mater. Chem. A* **2015**, *3*, 3868−3879.
(51) Jiang, J.; Swierk, J. R.; Hedstrom, S.; Matula, A. J.; Crabtree, R. H.; Batista, V. S.; Schmuttenmaer, C. A.; Brudvig, G. W. Molecular Design of Light-Harvesting Photosensitizers: Effect of Varied Linker Conjugation on Interfacial Electron Transfer. *Phys. Chem. Chem. Phys.* **2016**, *18*, 18678−18682.
(52) Rego, L. G. C.; Batista, V. S. Quantum Dynamics Simulations of Interfacial Electron Transfer in Sensitized TiO_2 Semiconductors. *J. Am. Chem. Soc.* **2003**, *125*, 7989−7997.
(53) Li, C.; et al. Facet-Dependent Photoelectrochemical Performance of TiO_2 Nanostructures: An Experimental and Computational Study. *J. Am. Chem. Soc.* **2015**, *137*, 1520−1529.
(54) Weigend, F.; Ahlrichs, R. Balanced Basis Sets of Split Valence, Triple Zeta Valence and Quadruple Zeta Valence Quality for H to Rn: Design and Assessment of Accuracy. *Phys. Chem. Chem. Phys.* **2005**, *7*, 3297−3305.
(55) Urbani, M.; Grätzel, M.; Nazeeruddin, M. K.; Torres, T. Meso-Substituted Porphyrins for Dye-Sensitized Solar Cells. *Chem. Rev.* **2014**, *114*, 12330−12396.
(56) Lindsey, J. S. Synthetic Routes to meso-Patterned Porphyrins. *Acc. Chem. Res.* **2010**, *43*, 300−311.
(57) Ladomenou, K.; Kitsopoulos, T. N.; Sharma, G. D.; Coutsolelos, A. G. The Importance of Various Anchoring Groups Attached on Porphyrins as Potential Dyes for DSSC Applications. *RSC Adv.* **2014**, *4*, 21379−21404.
(58) Ding, W.; et al. Linker Rectifiers for Covalent Attachment of Transition-Metal Catalysts to Metal-Oxide Surfaces. *ChemPhysChem* **2014**, *15*, 1138−1147.
(59) Imahori, H.; Hayashi, S.; Umeyama, T.; Eu, S.; Oguro, A.; Kang, S.; Matano, Y.; Shishido, T.; Ngamsinlapasathian, S.; Yoshikawa, S. Comparison of Electrode Structures and Photovoltaic Properties of Porphyrin-Sensitized Solar Cells with TiO_2 and Nb, Ge, Zr-Added TiO_2 Composite Electrodes. *Langmuir* **2006**, *22*, 11405−11411.
(60) Lindsey, J. S.; Schreiman, I. C.; Hsu, H. C.; Kearney, P. C.; Marguerettaz, A. M. Rothemund and Adler-Longo Reactions Revisited: Synthesis of Tetraphenylporphyrins Under Equilibrium Conditions. *J. Org. Chem.* **1987**, *52*, 827−836.
(61) Brennan, B. J.; Durrell, A. C.; Koepf, M.; Crabtree, R. H.; Brudvig, G. W. Towards Multielectron Photocatalysis: a Porphyrin Array for Lateral Hole Transfer and Capture on a Metal Oxide Surface. *Phys. Chem. Chem. Phys.* **2015**, *17*, 12728−12734.
(62) Chauhan, S. M. S.; Giri, N. G. Rosette Formation by Hydrogen Bonding of 5,5-dialkylbarbituric Acids with 2-amino-4,6-bis[5-(4′-aminophenyl)porphyrinatozinc]-1,3,5-triazines in Solution. *Supramol. Chem.* **2008**, *20*, 743−752.
(63) Khairutdinov, R. F.; Serpone, N. Photoluminescence and Transient Spectroscopy of Free Base Porphyrin Aggregates. *J. Phys. Chem. B* **1999**, *103*, 761−769.
(64) Regan, K. P.; Swierk, J. R.; Neu, J.; Schmuttenmaer, C. A. Frequency-Dependent Terahertz Transient Photoconductivity of Mesoporous SnO_2 Films. *J. Phys. Chem. C* **2017**, *121*, 15949−15956.
(65) Asbury, J. B.; Hao, E.; Wang, Y.; Lian, T. Bridge Length-Dependent Ultrafast Electron Transfer from Re Polypyridyl Complexes to Nanocrystalline TiO_2 Thin Films Studied by Femtosecond Infrared Spectroscopy. *J. Phys. Chem. B* **2000**, *104*, 11957−11964.

DOI: 10.1021/acs.jpcc.7b07855
J. Phys. Chem. C 2017, 121, 22690−22699

(66) Xiang, X.; Fielden, J.; Rodríguez-Córdoba, W.; Huang, Z.; Zhang, N.; Luo, Z.; Musaev, D. G.; Lian, T.; Hill, C. L. Electron Transfer Dynamics in Semiconductor−Chromophore−Polyoxometalate Catalyst Photoanodes. *J. Phys. Chem. C* **2013**, *117*, 918−926.
(67) Closs, G. L.; Miller, J. R. Intramolecular Long-Distance Electron Transfer in Organic Molecules. *Science* **1988**, *240*, 440.
(68) Yoshimori, A.; Kakitani, T.; Enomoto, Y.; Mataga, N. Shapes of the Electron-Transfer Rate vs Energy Gap Relations in Polar Solutions. *J. Phys. Chem.* **1989**, *93*, 8316−8323.
(69) Stubbe, J.; Nocera, D. G.; Yee, C. S.; Chang, M. C. Y. Radical Initiation in the Class I Ribonucleotide Reductase: Long-Range Proton-Coupled Electron Transfer? *Chem. Rev.* **2003**, *103*, 2167−2202.
(70) Gouterman, M.; Wagnière, G. H.; Snyder, L. C. Spectra of Porphyrins. *J. Mol. Spectrosc.* **1963**, *11*, 108−127.

DOI: 10.1021/acs.jpcc.7b07855
J. Phys. Chem. C 2017, 121, 22690−22699